Tang Wei (Orcid ID: 0000-0002-0912-7863)

Wei Tang (Orcid ID: 0000-0002-2662-217X)

Title: Phosphodiesterase-4 inhibition attenuates murine ulcerative colitis via interfering with mucosal immunity

Running title: PDE4 inhibition attenuates ulcerative colitis

Authors: Heng Li[1,2], Chen Fan[1], Chunlan Feng[1], Yanwei Wu[1], Huimin Lu[1,2], Peilan He[3], Xiaoqian Yang[3], Fenghua Zhu[3], Qing Qi[1], Yuanzhuo Gao[1,2], Jianping Zuo[2,3]*, Wei Tang[1,2]*

1 Laboratory of Anti-inflammation, Shanghai Institute of Materia Medica, Chinese Academy of Sciences, Shanghai 201203, China

2 School of Pharmacy, University of Chinese Academy of Sciences, Beijing 100049, China

3 Laboratory of Immunopharmacology, State Key Laboratory of Drug Research, Shanghai Institute of Materia Medica, Chinese Academy of Sciences, Shanghai 201203, China

* Correspondence. Wei Tang and Jianping Zuo, Shanghai Institute of Materia Medica, Chinese Academy of Sciences, Shanghai 201203, China. E-mail address: tangwei@simm.ac.cn and jpzuo@simm.ac.cn

Author contributions:

H.L., J.Z., and W.T. contributed to the conception and design of this study. H.L., C.F., CL.F., Y.W., HM.L., P.L., X.Y., F.Z., Q.Q., and Y.G. performed the experiments. H.L. and W.T. analyzed the data and wrote the manuscript. All the authors contributed to the interpretation of data and approved the final draft.

This article has been accepted for publication and undergone full peer review but has not been through the copyediting, typesetting, pagination and proofreading process which may lead to differences between this version and the Version of Record. Please cite this article as doi: 10.1111/bph.14667

Acknowledgements

This work was supported by grants from the National Science & Technology Major Project "Key New Drug Creation and Manufacturing Program", China (2018ZX09711002-006-011) and the "Personalized Medicines-Molecular Signature-based Drug Discovery and Development", Strategic Priority Research Program of the Chinese Academy of Sciences, Grant No. XDA12020231. We are kindly grateful for the credible pathological analysis from Center for Drug Safety Evaluation and Research, Shanghai Institute of Materia Medica (SIMM), Chinese Academy of Sciences (CAS) and technical assistance from the Platform of Molecular Imaging and Research, SIMM, CAS.

Conflict of interest statement

The authors declared that the manuscript was conducted in the absence of any commercial or financial relationships that could be construed as a potential conflict of interest.

Declaration of transparency and scientific rigour

This Declaration acknowledges that this paper adheres to the principles for transparent reporting and scientific rigour of preclinical research recommended by funding agencies, publishers and other organisations engaged with supporting research.

Abstract:

Background and purpose:

Ulcerative colitis (UC) is an etiologically refractory inflammatory disease, accompanied by dysfunction of epithelial barrier and intestinal inflammation. PDE4 serves as an intracellular proinflammatory enzyme targeting for degradation of cAMP. Though PDE4 inhibitors have been approved for pulmonary and dermatological diseases, the role of PDE4 inhibition in modulating mucosal immunity remains elusive. This study was designed to explore whether PDE4 inhibition by apremilast exerts protective effects in DSS-induced murine UC.

Experimental approach:

Intestinal inflammation and disease severity were evaluated by morphological, histopathological, biochemical assay and *in vivo* imaging examination. Expression of

inflammatory mediators, components of PDE4-mediated pathways in colon and macrophages were determined using quantitative real-time PCR, ELISA, Luminex assay, immunostaining or western blot, along with SiRNA knockdown. Immune cells in mesenteric lymph nodes and colonic lamina propria were analyzed by flow cytometry.

Key results:

Apremilast significantly attenuated clinical features of UC, as shown by suppression of microscopic colon damage, inflammatory mediators production, oxidative stresses and fibrosis. Apremilast also promoted epithelial barrier function and inhibited infiltration of immune cells to the inflamed tissues, through decreasing expression of chemokines and chemokine receptors. Furthermore, in UC, PDE4A, PDE4B, PDE4D were observed to highly express in colon and apremilast not only inhibited PDE4 isoforms expression, but also activated PKA-CREB and Epac-Rap1 pathway and subsequently suppressed MAPK, NF-κB, PI3K-mTOR, and JAK-STAT-SOCS3 activation.

Conclusion and implications:

PDE4 inhibition by apremilast exerted protective effects in UC via interfering with mucosal immunity, which represented a promising strategy for regulating intestinal inflammation.

Keywords: PDE4, apremilast, ulcerative colitis, mucosal immunity, epithelial integrity

Abbreviations：

BMDM, bone marrow derived macrophages; CREB, cAMP-response element binding protein; cAMP, cyclic adenosine monophosphate; DAI, disease activity index; DSS, dextran sulfate sodium; IBD, inflammatory bowel disease; LPS, lipopolysaccharide; MLN, mesenteric lymph node; MMP, matrix metalloproteinase; MPO, myeloperoxidase; PDE4, phosphodiesterase 4; PKA, protein kinase A; ROS, reactive oxygen species; TEER, trans-epithelial electrical resistance; UC, ulcerative colitis.

Bullet point summary:

'What is already known': Clinical trials of the PDE4 inhibitor, apremilast, on UC are ongoing.

'What this study adds': This study illustrates the pathological role of PDE4 in intestinal inflammation.

'Clinical significance': PDE4 inhibition by apremilast represents a potential therapeutic strategy for UC patients.

Introduction

Inflammatory bowel diseases (IBD), including ulcerative colitis (UC) and Crohn's disease (CD) are etiologically idiopathic, chronic, relapsing, refractory inflammatory conditions that refer to the interaction of gene susceptibility, environmental factors, disturbance of immune homeostasis and microbiological anomaly in the gastrointestinal tract (Sartor, 2006). In the past decade, UC has bloomed to become a global health challenge with the great prevalence of over 0.3% worldwide (Ng *et al.*, 2018). UC can present in patients with life-altering syndromes lasting weeks to months, such as diarrhea, bleeding, abdominal pain, fecal urgency and severe fever. Recently, in addition to a wide spectrum of therapeutic corticosteroids, immunosuppressants, and biological drugs, phosphodiesterase 4 (PDE4) inhibitors have also shown dramatic therapeutic efficacies for the treatment of UC symptoms (Spadaccini *et al.*, 2017).

PDE4 family is the main isoenzyme in diverse immune cells and epithelial cells (Chiricozzi *et al.*, 2016). PDE4 is highly specific for cAMP degradation and elevation of intracellular cAMP by PDE4 inhibition contributes to suppression of cell trafficking, chemokines and cytokines release from inflammatory cells. Decrease of colon cAMP and upregulation of PDE4 expression were observed in IBD, which resulted in abnormal production of cytokines in the inflamed intestine (Banner *et al.*, 2004; Schafer *et al.*, 2016). Given the suppression of inflammatory cytokines upon PDE4 inhibition, rolipram, tetomilast and roflumilast have been applied in the experimental models of colitis (Hartmann *et al.*,

2000; Ichikawa *et al.*, 2008; El-Ashmawy *et al.*, 2018). Although these inhibitors showed therapeutic effects in acute or chronic colitis, the adverse effects have impeded further clinical application.

In contrast with the transmural and widespread throughout the entire gastrointestinal tract, inflammation present in CD, inflammation in UC is primarily limited in the mucosal and submucosal layers of the colon (Sartor, 2006). Although the delicate pathogenesis of UC remains enigmatic, disturbed mucosal immune homeostasis and destruction of epithelial integrity are deemed to be critical to the initiation and perpetuation of UC (Banner *et al.*, 2004; Xu *et al.*, 2014). Pathogens that gain access to lamina propria following the destruction of epithelial integrity and manage to expand out of control pose a critical risk factor of UC (Cader *et al.*, 2013; Boyapati *et al.*, 2016). Under inflammatory conditions, certain activated immune cells infiltrate into the colonic mucosa, which result in high level of inflammatory cytokines, chemokines, and adhesion molecules, along with redundant expression of chemokine receptors and integrin. Macrophages and DCs plays a vital role in the aggravation of UC and function conventionally as the antigen-presenting cells priming naïve T cells and resulting in differentiation into inflammatory phenotypes (Steinbach *et al.*, 2014). Furthermore, there is a substantial increase in the pathological T cells responses, which are pathologically responsible for abnormal expression of various tight-junction proteins and subsequent persistence of mucosal inflammation (de Mattos *et al.*, 2015).

The PDE4 inhibitor apremilast, approved in 2014, represent a breakthrough and blessedness for patients with psoriasis and psoriatic arthritis (Schafer *et al.*, 2010; Chiricozzi *et al.*, 2016). Apremilast is a well-tolerated PDE4 inhibitor with mild-to-moderate adverse effects. Besides, apremilast has also been applied clinically in other inflammatory disorders, such as Behcet's Syndrome (BS), ankylosing spondylitis (AS), frontal fibrosing alopecia and discoid lupus erythematosus (Li *et al.*, 2018). However, there have been none preclinical research on inflammatory colitis published by now. Hence, we aimed to explore whether apremilast exert protective effects in intestinal inflammation. on DSS-induced murine acute colitis, in the present study, the dextran sulfate sodium (DSS) induced colitis was used to test

our hypothesis.

Methods

DSS-induced colitis and drug treatment

Animal studies are reported in compliance with the ARRIVE guidelines (Kilkenny *et al.*, 2010; McGrath *et al.*, 2015). All experiments were carried out according to the National Institutes of Health Guide for Care and Use of Laboratory Animals and were approved by the Bioethics Committee of the Shanghai Institute of Materia Medica (SIMM). Wide-type male C57BL/6J mice (8 weeks, 22-24g, RRID: IMSR_JAX:000664) were purchased from Shanghai Lingchang Biotechnology Co., Ltd. (Certificate No.2013-0018, China). The mice were housed under specific pathogen-free conditions with 12 h of light/12 h of dark cycle, 22±1 °C and 55±5% relative humidity. All mice were fed standard laboratory chow and water ad libitum and allowed to acclimatize in our facility for one week before any experiments started.

Mice were randomly divided into three groups consisting of normal, vehicle (only DSS), and treatment (DSS+Apremilast) group with 8 mice per group. Ulcerative colitis was induced by administration of 3% DSS for 7 days and further drinking water taken for another 4 days as previously reported (Chassaing *et al.*, 2014). Apremilast (50 $mg \cdot kg^{-1}$) were dissolved in 0.5 % carboxymethylcellulose sodium and 0.25 % Tween 80 and orally administrated once daily. During the treatment, weight loss, stool consistency and fecal blood, as indicators of disease activity index (DAI), were monitored by 3 investigators who were blinded to the experimental conditions. The DAI scores were calculated as the sum of the weight loss, stool consistency and rectal bleeding score shown in Table1 adapted from previous description (Wirtz *et al.*, 2017). On day 11, mice were anesthetized with an intraperitoneal injection of 4% chloral hydrate and the serum samples were collected for biochemical indexes assay using a HITACHI-7080 automatic biochemical analyzer (Hitachi High Technologies Corporation, Tokyo, Japan). The spleen, mesenteric lymph nodes and colons were collected for following assessment.

Histopathological examination

Colon sections were taken and length of the colon from the anus to appendix was measured by a ruler. The sections for histological examination were fixed in 10% phosphate-buffered saline (PBS)-buffered formalin at room temperature, and then embedded in paraffin. Sections measuring 5 μm were cut and stained with hematoxylin and eosin (H&E). For colon fibrosis, slices were stained with Masson′s trichrome reagents. Histopathological features were observed under a light microscope and scored by 3 investigators who were blinded to the experimental conditions in the Center for Drug Safety Evaluation and Research, SIMM, Chinese Academy of Sciences (CAS), which are authoritative under Good Laboratory Practice (GLP). The scoring standards were shown as following: 0, no evidence of inflammation; 1, low level inflammation with scattered mononuclear cells (1-2 foci); 2, moderate inflammation with multiple foci of mononuclear cells; 3, high level inflammation with increased vascular density and marked wall thickening; and 4, maximal inflammation with transmural leukocyte infiltration and loss of goblet cells.

MPO, SOD and MDA measurement

Freshly excised colon was rinsed with PBS, homogenized in tissue lysis buffer and centrifuged. Individual activities of MPO, SOD and MDA was determined using an MPO activity assay kit (Nanjing Jiancheng Bioengineering Institute, China), SOD assay kit (Beyotime, Haimen, China) and MDA assay kit (Beyotime) according to the manufacturer's instructions. MPO activity was defined as the quantity of enzyme degrading 1 $\mu mol \cdot ml^{-1}$ peroxide at 37˚C and expressed as $U \cdot mg^{-1}$ of colon protein. SOD and MDA activity were expressed as $U \cdot mg^{-1}$ colonic protein and $mol \cdot mg^{-1}$ colonic protein.

***In vivo* imaging and intestinal permeability measurement**

The luminol-based chemiluminescent probe L-012 was applied to determine the intestinal inflammation. On the day of *in vivo* imaging, start the Living Image software and initialize the IVIS Spectrum CT system according to the manufacturer's instructions (Kielland *et al.*, 2009). Briefly, mice were anesthetized in a chamber with 1.5-2.0% isoflurane, injected intraperitoneally with 25 $mg \cdot kg^{-1}$ L-012 solution and were placed in a supine position into the

anesthesia manifold in the imaging chamber of the IVIS Spectrum CT bioluminescence imaging system. The bioluminescent images were acquired 1 min after injection using the autoexposure option to automatically regulate acquisition parameters (shutter speed, binning and aperture of the system) to optimize signal intensity (Wirtz *et al.*, 2017).

For intestinal permeability assay, mice were fasted overnight and FITC-dextran solution (3-5 kDa, 600 $mg \cdot kg^{-1}$) were orally dosed with a syringe through a blunt-ended curved feeding tube. After 4 h administration, mice were anesthetized and the blood samples were harvested via cardiac puncture. Blood were then centrifuged at 10000 rpm and 4 ℃ for 10 min and the fluorescence intensity of FITC in serum were measured at 480 nm excitation and 520 nm emission using a microplate reader. Meanwhile, mice were exposed to the IVIS Spectrum CT system and the fluorescent images were acquired at 480 nm excitation and 520 nm emission to determine the retention of FITC-dextran in the abdominal region (Gupta *et al.*, 2014).

Full-thickness colonic tissue culture

The longitudinal 1-cm segments of the colon were isolated at the same region using surgical forceps and scissors as described previously (Wirtz *et al.*, 2017). The colonic segments were washed with cold PBS, cut into three or four defined biopsies and then cultured for 24 h containing 0.5 ml of sterile cell culture medium at 37 ℃ in a humidified incubator of 5% CO_2. The supernatants were collected and determined for cytokines production.

Flow cytometry assay

Mesenteric lymph nodes and spleen were extracted from the mice using sterile technique and dissected mechanically. Mononuclear splenocytes suspensions were prepared after cell debris, and clumps were removed. Erythrocytes were depleted with ammonium chloride buffer solution. Cells were washed once with fresh medium and were filtered using a 70 μm filter to obtain a mononuclear cell suspension. Cells from the colonic lamina propria (LP) were isolated as described (Uhlig *et al.*, 2006). Colons were cut into small pieces and incubated in RPMI 1640 containing 10% FBS and 5 mM EDTA for 15 min in a shaking incubator at 37 ℃

for three times to remove epithelial cells. The remaining tissue was digested using RPMI 1640 containing 10% FBS, 0.5 mg·ml^{-1} Type Ⅳ Collagenase, 3 mg·ml^{-1} Dispase Ⅱ and 0.1 mg·ml^{-1} DNase Ⅰ for 30 min in a 37°C shaking incubator. LP cells were collected and filtered using a 70 μm filter to obtain a mononuclear cell suspension.

Single cell suspensions were washed with phosphate buffered saline (PBS) and then stained with fixable viability dye eFluor™ 780 (eBioscience, San Diego, CA, USA) for 30 min at 4 ℃ to identify viable cells from the dead cells. Following, cells were blocked with anti-CD16/CD32 mAb (Thermo Fisher Scientific Cat# 14-0161-86, RRID: AB_467135) and stained with brilliant ultraviolet 395 (BUV395)-conjugated CD45 (BD Biosciences Cat# 564279, RRID: AB_2651134), fluorescein isothiocyanate (FITC)-conjugated anti-CD62L (BD Biosciences Cat# 553150, RRID: AB_394665), FITC-conjugated anti-γδTCR (Thermo Fisher Scientific Cat# 11-5711-82, RRID: AB_465238), FITC-conjugated anti-CD4 (BD Biosciences Cat# 553651, RRID: AB_394971), FITC-conjugated anti-Gr-1 (Thermo Fisher Scientific Cat# 11-5931-81, RRID: AB_465313), FITC-conjugated anti-CD8 (BD Biosciences Cat# 551347, RRID: AB_394159), phycoerythrin (PE)-conjugated anti-CD25 (BD Biosciences Cat# 553866, RRID: AB_395101), PE-conjugated anti-F4/80 (BD Biosciences Cat# 565410, RRID: AB_2687527), Peridinin-chlorophyll proteins-Cyanine5.5 (Percp-Cy5.5)-conjugated anti-CD44 (Thermo Fisher Scientific Cat# 45-0441-80, RRID: AB_925747), Percp-Cy5.5-conjugated anti-CD11b (BD Biosciences Cat# 550993, RRID: AB_394002), Percp-Cy5.5-conjugated anti-CD4, allophycocyanin (APC)-conjugated anti-CD11c (BD Biosciences Cat# 550261, RRID: AB_398460), APC-conjugated anti-CD4 (BD Biosciences Cat# 553051, RRID: AB_398528) and brilliant violet 421 (BV421)-conjugated anti-CD3 (BD Biosciences Cat# 564008, RRID: AB_2732058). For intracellular staining, cells were stained with surface markers, followed by fixation and permeabilization using Foxp3 Staining Buffer set (Thermo Fisher Scientific, MA, USA). Cells were labelled intracellularly with PE-conjugated anti-IL-17A (BD Biosciences Cat# 559502, RRID: AB_397256) and Percp-Cy5.5-conjugated anti-Foxp3 (Thermo Fisher Scientific Cat# 45-5773-82, RRID: AB_914351). All immunofluorescent antibodies used in

this research were obtained from BD Biosciences (Franklin Lakes, NJ, USA) or Thermo Fisher Scientific (Waltham, MA, USA). The data were analyzed using FlowJo software (RRID: SCR_008520, Tree Star, Ashland, OR, USA).

***ex vivo* proliferation and cytokines production**

Mesenteric lymph nodes cells from three groups were prepared, and stimulated with anti-CD3 antibodies (5 $\mu g \cdot ml^{-1}$, Thermo Fisher Scientific Cat# 14-0031-81, RRID: AB_467048) and LPS (10 $\mu g \cdot ml^{-1}$), respectively. After incubation, the cultures were pulsed with 0.5 $\mu Ci \cdot well^{-1}$ [^{3}H-TdR] thymidine to determine cells proliferation activity and the supernatants were collected to determine the cytokine levels.

Polyclonal $CD4^+$ T cells were isolated from mesenteric lymph nodes cells using EasySep™ mouse $CD4^+$ T Cell isolation kit (Stemcell, Vancouver, BC, Canada) according to the manufacturer's instructions, respectively. To acquire $CD4^+$ T cells, immunomagnetic negative selection were performed for removal with biotinylated antibodies recognizing specific cell surface markers. Unwanted cells ($CD8^+$ cells, $B220^+$ cells, $CD11b^+$ cells, and $I\text{-}A^+$ antigen presenting cells from splenocytes) were separated with an EasySep™ magnet. The purity of the $CD4^+$ T cells was consistently >98% determined by flow cytometry. Purified $CD4^+$ T cells were cultured with medium alone or anti-CD3 antibodies (5 $\mu g \cdot ml^{-1}$) and anti-CD28 antibodies (2 $\mu g \cdot ml^{-1}$, Thermo Fisher Scientific Cat# 14-0281-86, RRID: AB_467192). After incubation, the cell cultures were pulsed with 0.5 $\mu Ci \cdot well^{-1}$ [^{3}H-TdR] thymidine to determine $CD4^+$ T cells proliferation activity and the supernatants were collected to determine the cytokine levels.

Cell cultures and treatment

Murine adherent macrophage cell line RAW264.7 cells (ATCC Cat# TIB-71, RRID: CVCL_0493) and human adherent epithelial cell line Caco-2 cells (ATCC Cat# HTB-37, RRID: CVCL_0025) were purchased form American Type Culture Collection (ATCC, Manassas, VA, USA). RAW264.7 cells were grown in DMEM containing 10% FBS, 2 $mmol \cdot L^{-1}$ L-glutamine, 100 $U \cdot mL^{-1}$ penicillin, and 100 $\mu g \cdot mL^{-1}$ streptomycin. Caco-2 cells were grown in DMEM containing 10% FBS, 2 $mmol \cdot L^{-1}$ L-glutamine, 100 $U \cdot mL^{-1}$ penicillin,

and 100 μg·mL^{-1} streptomycin. The cells were maintained at 37 ℃ in a humidified incubator of 5% CO_2. For epithelial barrier function assay, Caco-2 cells were seeded on collagen-coated polycarbonate membrane transwell support (Corning Costar, Acton, MA). The cell monolayers were incubated with or without 10 ng·ml^{-1} TNF-α and 10 ng·ml^{-1} IFN-γ in the absence or presence of different concentrations of apremilast for 72 h. The electrical resistance of the filter-grown monolayers was measured by using an EVOM volt ohmmeter (EVOM, Hertfordshire, England) with a pair of STX-2 chopstick electrodes (WPI, Sarasota, Florida, USA). Then FITC-labeled dextran was added to the apical side of the monolayer and after 2h incubation, FITC-dextran fluorescence was measured using a microplate reader.

Bone marrow-derived macrophages (BMDMs) were obtained from the femur and tibia bones of 6-week old of C57BL/6J mice as previously described (Ying *et al.*, 2013). BMDMs were cultured for 7 days in Iscove's Modified Dulbecco's Medium (IMDM) containing 10% FBS and 10 ng·ml^{-1} of mouse colony-stimulating factor (M-CSF). To detach and resuspend mature macrophages after differentiation, 5 mM EDTA in Ca^{2+} and Mg^{2+}-free Hank's balanced buffer (HBSS) were used and then the purity of mature macrophages was consistently >98%, defined as the percentage of $CD11b^{+}F4/80^{+}$ populations by flow cytometry analysis.

BMDMs and RAW264.7 cells were treated with different concentrations of apremilast in the absence or presence of LPS. The supernatants were collected for cytokines detection, meanwhile, cells were centrifuged and then detected for western blot assay and immunofluorescence for phosphor-CREB. To investigate the critical role of PKA-CREB in the anti-inflammation, BMDMs and RAW264.7 cells were incubated with 10 μM H89 (PKA inhibitor) or 10 μM Forskolin (adenylate cyclase activator), then the cells and supernatants were collected for determining cytokines production and phosphorylation of CREB.

SiRNA transfection

To knock-down the PKA expression in BMDMs and RAW264.7 cells, siRNA targeting for PKA C-α silence (CST, Danvers, MA, USA) were used following the manufacturer′ instructions. Briefly, cells were transfected with siRNA, mixed with Lipofectamine®

RNAiMAX Reagent (Thermo Fisher Scientific, Waltham, MA, USA) in serum-free opti-MEM medium. Cells were collected and detected for PKA C-α expression after 72 h of transfection. The percentage of knockdown for PKA C-α is over 80%.

cAMP measurements

Briefly, 50-80% confluence of RAW264.7 and BMDMs were treated at the indicated concentrations of apremilast, H89 and Forskolin for 30 min. Cells were harvested, lysed by 0.1 M HCl, and then centrifuged for supernatant collection. Intracellular cAMP was assayed with the direct cAMP ELISA kit purchased from Enzo Life Sciences (Raamsdonksveer, The Netherlands) according to the manufacturer's instruction. The content of cAMP was expressed as pmol cAMP per mg of total protein to normalize for protein content (The Units were expressed as pmol·mg^{-1} protein).

Cytokines detection

Quantification of cytokines in serum was performed using the Luminex x-MAP technology (Luminex Corp, Austen TX, USA). Serum from colitis mice were analyzed using a Milliplex multi-analyte magnetic bead panel obtained from Thermo Fisher Scientific (Waltham, MA, USA) and all data were collected on a Luminex 200 instrument. All standard curves with four-parameter logistic fitting generated from the known cytokine concentrations supplied by the manufacturer had R^2 values calculated at or close to 1 and quality controls in the kit performed as expected.

Cytokines in colon homogenates and culture supernatants were determined by using mouse TNF-α, IFN-γ, IL-1β, IL-2, IL-6, IL-10, IL-12p40, and IL-17A ELISA kits (BD Pharmingen, San Diego, CA, USA) according to the manufacturer's instructions.

Immunohistochemistry and immunofluorescence

Formalin-fixed paraffin-embedded tissues were sectioned at 5 μm and collected onto coherent glass slides. Tissue sections were dewaxed in xylene and rehydrated through graded alcohol to water. Endogenous peroxidase activity was blocked with 3% hydrogen peroxide before masked antigens were retrieved by 0.01M citrate buffer solution. For immunohistochemistry, the sections were blocked with 10% normal horse serum and

incubated overnight at 4 °C in a humidified environment with PDE4D (Proteintech Group Cat# 12918-1-AP, RRID: AB_2161097, Rosemont, USA) and phosphor-p65 (Cell Signaling Technology Cat# 3033), phosphor-ERK (Cell Signaling Technology Cat# 4376, RRID: AB_331772, Danvers, MA, USA). Primary labeling was detected using biotinylated horse anti-rabbit IgG secondary antibody, incubated with streptavidin-horseradish peroxidase and then signals were detected using diaminobenzidine. For immunofluorescence, the tissue sections were blocked with 10% normal horse serum and incubated overnight at 4 °C in a humidified environment with Alexa Fluor 488-conjugated anti-E-cadherin (Cell Signaling Technology Cat# 3199, RRID: AB_10691457), FITC-conjugated CD11b (Abcam Cat# ab18273, RRID: AB_444372, Cambridge, MA, USA), Alexa Fluor 647-conjugated F4/80 (Abcam Cat# ab204467), Alexa Fluor 647-conjugated Ly6G (BioLegend Cat# 127609, RRID: AB_1134162, San Diego, CA, USA), FITC-conjugated CCR5 (Abcam Cat# ab11466, RRID: AB_2275506), CXCR3 (Proteintech Cat# 26756-1-AP, Rosemont, USA), ZO-1 (Proteintech Cat# 21773-1-AP) and Epac1 (Cell Signaling Technology Cat# 4155). Primary labeling for unconjugated fluorescein was detected using FITC-conjugated secondary antibodies and then counterstained with DAPI and mounted in N-propyl gallate in glycerol-PBS. Images were collected on Leica TCS SPS microscope.

RNA extraction, cDNA synthesis, and qPCR

Total RNA was extracted from colon tissue by using RNAsimple total RNA kit (Tiangen, Beijing, China) and then reverse transcribed by an All-in-One cDNA Synthesis SuperMix (Biotool, Houston, TX, USA). Real-time PCR was performed with SYBR® Green Realtime PCR Master Mix (TOYOBO, Osaka, Japan) on an Applied Biosystems 7500 Fast Real-Time PCR System (Applied Biosystems, Foster city, CA, USA). The primers used for PCR amplification are listed in Supporting Table S1. The fold change in mRNA expression of gene was normalized to β-actin using the $\Delta\Delta$ Ct method.

Western Blotting

Cells and colon samples were lysed with sodium dodecyl sulfate sample buffer and protein concentration was determined by the Pierce BCA protein assay kit (Thermo Fisher Scientific, Waltham, MA, USA). Equal amounts of protein (10-30 μg) were subjected to 10% SDS-PAGE and transferred to a nitrocellulose membrane (Bio-Rad, Hercules, CA, USA). Nonspecific binding was blocked with 5% BSA and the membranes were incubated overnight (4 ℃) with rabbit or mouse primary antibodies (Supporting Information Table S2). Signals were detected with HRP-conjugated anti-rabbit IgG (1:20000) or HRP-conjugated anti-mouse IgG (1:10000) using SuperSigna West Femto Maximum Sensitivity Substrate under visualization in a ChemiDoc™ MP Imaging System (Bio-Rad).

Data and analysis

The data and statistical analysis comply with the guidance on experimental design and analysis in pharmacology (Curtis *et al.*, 2015) and its update (Curtis *et al.*, 2018). All the images of Western blots and immunohistochemistry (stainings) were quantified using Image-Pro Plus software (RRID: SCR_007369, Media Cybernetics, Silver Springs, MD, USA). All experimental data are presented as mean ± SEM, and each experiment was performed a minimum of three times. All group data subjected to statistical analysis in the present research have a minimum of n=5 individuals per group or independent samples according to the power analysis in pharmacology (Curtis *et al.*, 2015). Statistical analyses were evaluated using GraphPad Prism 6.0 software (RRID: SCR_002798, La Jolla, CA, USA). Significant differences between groups were determined using a one-way ANOVA with Dunnet's multiple comparisons test with no significant variance inhomogeneity (F achieved $p<0.05$) and $p<0.05$ was considered to represent a significant difference.

Materials

Except where indicated, all the materials and reagents were obtained from Sigma (St Louis, MO, USA). Dextran sulfate sodium (DSS, molecular weight 36-50 kDa) was purchased from MP Biomedicals (Irvine, CA, USA). Apremilast (M.W.=460.5) was purchased from Selleck (Shanghai, China). The fecal occult blood test kits were obtained from the Nanjing Jiancheng Bioengineering Institute (Nanjing, China). Anti-CD3 and CD28 antibodies were purchased from Thermo Fisher Scientific (Waltham, MA, USA). CCK-8 (Cell Counting Kit-8) was purchased from Dojindo (Kumamoto, Japan).

Nomenclature of Targets and Ligands

Key protein targets and ligands in this article are hyperlinked to corresponding entries in http://www.guidetopharmacology.org, the common portal for data from the IUPHAR/BPS Guide to PHARMACOLOGY (Harding *et al.*, 2018), and are permanently archived in the Concise Guide to PHARMACOLOGY 2017/18 (Alexander *et al.*, 2017).

Results

Apremilast ameliorated DSS-induced ulcerative colitis in mice

The DSS-induced mouse model of colitis is well-characterized by increased colon ulceration and acute inflammation. Mice with colitis exhibited body weight loss from nearly day 5 onward; and diarrhea and rectal bleeding appeared upon DSS application (Figure 1A). Compared to the vehicle controls, apremilast-treated colitic mice showed a prominent reduction in body weight loss and DAI scores during the disease progression in a dose-dependent manner (Figure 1A and Supporting Information Figure S1A, S1B). Splenomegaly was associated with colitis and apremilast obviously suppressed the spleen index presented as the ratio of spleen to body weight (Figure 1B and Supporting Information Figure S1C). In addition, shorting of colon caused by inflammation was an experimental indicator of colitis and apremilast dose-dependently increased colon length in contrast to the vehicle mice (Figure 1C, D and Supporting Information Figure S1D, S1E). It's worth mentioning that the mice only treated with apremilast exhibited no inflammation and

manifested with no symptoms of diarrhea, splenomegaly and colon shortening (Supporting Information Figure S1A-E). Considering the therapeutic effects of two dosage strategies, we present the following readouts from 50 $mg \cdot kg^{-1}$ apremilast treated colitic mice.

We next determined the serum level of clinical biochemical indexes in colitis. Due to excessive bleeding and metabolic disturbance, DSS-treated mice showed decreased serum ALB, ALP and increased TG and TC. Interestingly, to some extent, apremilast restored the level of biochemical indexes (Figure 1E). Furthermore, the results of serum cytokines by Luminex assay showed that apremilast markedly inhibited the inflammatory cytokines secretion, including TNF-α, IFN-γ, IL-1β, IL-2 and IL-6, compared to the vehicle group (Figure 1F). The severity of colonic inflammation was further evaluated by histopathological analysis. In the DSS-treated mice, colon tissue presented obvious mucosal ulceration, loss of crypt, goblet cells and epithelium damage, and neutrophils infiltration (Figure 1H). By contrast, apremilast treatment received a dramatic improvement in histological damage (Figure 1G, H).

Apremilast suppressed the oxidative stress responses in DSS-colitis

MPO, SOD and MDA play key roles in oxidative stress responses and inflammation. It was observed that under exposure to DSS induction, the levels of MPO and MDA in serum and colonic tissue homogenates were much higher, while the levels of SOD lower than normal controls (Figure 1I, J). The abnormal serum and colon levels of MPO, SOD and MDA were significantly restored upon apremilast treatment (Figure 1I, J). Besides, reactive oxygen species (ROS) are implicated in oxidative damage and tissue dysfunction. Both in the spleens and mesenteric lymph nodes (MLNs), apremilast decreased DSS-induced upregulation of ROS (Figure 1K), which were mainly derived from $CD8^+$ T cells (Supporting Information Figure S2).

Apremilast inhibited the inflammatory responses and tissue fibrosis in colon

To evaluate the inflammatory conditions within the gut microenvironment, we determined the cytokines production in the supernatant of full-thickness colon tissue culture. As shown in Figure 2A, inflammatory mediators were suppressed in the colon cultures of apremilast-treated mice in comparison with DSS controls, such as TNF-α, IFN-γ, IL-6, IL-12p40 and IL-17A. Correspondingly, the cytokines profile in colonic homogenates showed that the protein levels of TNF-α, IFN-γ, IL-1β, IL-2, IL-6, and IL-17A in apremilast-treated group were much lower than those in vehicle controls, while IL-10 was upregulated mildly in apremilast-treated group (Figure 2B). Further analyses of mRNA expression of cytokines in colon confirmed the therapeutic effects of apremilast on colon inflammation (Figure 2C). Moreover, apremilast treatment resulted in a reduction of the mRNA levels of iNOS, COX-2 (Figure 2D) and inflammasome-associated genes, including NLRP3 and IL-18, with none effects on ASC and caspase-1 expression (Figure 2E).

Intestinal fibrosis is a common complication of IBD, which develops through various immune cells, extracellular matrix, cytokines abnormal production and collagen deposition (Suzuki *et al.*, 2011; Speca *et al.*, 2012). Previously, it has been reported that during the progression of DSS-induced colitis, fibrosis could be observed after 6 days of DSS exposure (Suzuki *et al.*, 2011). Histopathological examination of colon fibrosis demonstrated that first signs of fibrotic lesions were observed in the colonic mucosa and submucosa (Figure 2F). Apremilast showed a reduction of collagen deposition and suppressed the expression of genes related to fibrosis, including Col1a1, oncostatin M (OSM) and its receptor (OSMR), podoplanin (PDPN), and fibroblast activation protein (FAP) (Figure 2F, G).

Apremilast protected the intestinal epithelial barrier function in DSS-colitis

The intestinal epithelial integrity serves as the fundamental barrier against exogenous antigens and damage. Therefore, the present study evaluated the effects of apremilast on intestinal barrier function using *in vivo* imaging of inflammation with L-012 solution and FITC-dextran. It was observed that severe inflammation appeared in the location of intestinal tract in DSS-induced colitis mice and apremilast decreased the positive signals under L-012

injection (Figure 3A). When orally administrated, FITC-dextran was primary discharged through the intestinal and urinary systems and the gut-transit time affected the movement of FITC-dextran along the digestive tract (Wang *et al.*, 2015; Woting *et al.*, 2018). Once intestinal injury and inflammation occurred, intestinal retention and blood penetration of FITC-dextran increased obviously (Figure 3B). The green fluorescent images by IVIS spectrum indicated that apremilast-treated colitic mice showed much lower retention than DSS-treated mice (Figure 3B, left). Consistently, after absorption, distribution and metabolism, the serum fluorescence intensity of FTIC-dextran in apremilast-treated mice was apparently lower than that in DSS-treated mice (Figure 3B, right and Supporting Information Figure S1F, S1G). Moreover, there was no change of intestinal permeability in normal mice treated with apremilast (Supporting Information Figure S1F, S1G). To verify the involvement of epithelial tight junctions, we further examined the expression of colonic tight junction protein, such as ZO-1, E-cadherin and occludin, using immunofluorescence, western blot and quantitative real-time PCR (RT-qPCR). Apremilast protected the intestinal epithelial barrier well, meanwhile, both the protein and mRNA levels of ZO-1, E-cadherin and occludin were also evidently reversed (Figure 3C, E). Further staining results showed that the epithelial integrity in vehicle controls was destructed, manifesting with great loss of ZO-1 and E-cadherin *in situ* expression (Figure 3D). Additionally, apremilast inhibited the expression of matrix metalloproteinase-2 (MMP2), MMP3 and MMP9 in the colon (Figure 3F).

Apremilast prevented cytokines-induced integrity disruption and permeability *in vitro*

To validate the effects on epithelial barrier, we analyzed the protective efficacies of apremilast against pro-inflammatory cytokines-induced barrier dysfunction. TNF-α and IFN-γ synergize to reduce the trans-epithelial electrical resistance (TEER) and increase the paracellular permeability of Caco-2 cell monolayers *in vitro* (Figure 3G, H). Our results revealed that apremilast could potentially prevent the decrease of TEER and increase of paracellular permeability in a concentration-dependent manner (Figure 3G, H). In the following investigations of ZO-1 morphology and subcellular distribution, the tight junction ZO-1 localized at the apical cellular junctions and formed a dense reticular structure at the

cellular borders (Figure 3I, J). TNF-α plus IFN-γ stimulation caused desultory localization and irregular ring structures of membrane, while apremilast markedly attenuated the ZO-1 impairment of Caco-2 cells (Figure 3I, J).

Apremilast suppressed the leukocytes infiltration accompanying with chemokines and receptors expression

The abnormal interaction and crosstalk between mesenteric lymph nodes (MLN) and gut lamina propria provide the pathogenicity in the initiation and progression of UC (Cader *et al.*, 2013). To gain insights into the pathological role of mucosal immunity in the intestine, MLN and colonic lamina propria immune cells populations were isolated and analyzed by flow cytometry (Supporting Information Figure S3). The severity of DSS-induced colitis was closely associated with an increase in leukocytes proportions. As observed both in the MLN (Figure 4A) and lamina propria (Figure 4C), monocytic myeloid cells, macrophages, neutrophils and dendritic cells were increased in DSS-treated mice, which were reversed in the apremilast groups. Immune cell infiltrations were verified in immunofluorescence staining with CD11b, F4/80 and Ly6G, which mainly scattered across the mucosal layers of colon (Figure 4E). In addition, apremilast decreased the percentage of $CD44^{+}CD62L^{-}$ (gated on $CD3^{+}CD4^{+}$), $CD4^{+}IL\text{-}17^{+}$ (gated on $CD3^{+}$) and increased the percentage of $CD44^{-}CD62L^{+}$ (gated on $CD3^{+}CD4^{+}$), $CD25^{+}Foxp3^{+}$ (gated on $CD3^{+}CD4^{+}$) (Figure 4B). Correspondingly, apremilast suppressed the infiltration of $\gamma\delta TCR^{+}$, $CD4^{+}$, and $CD8^{+}$ T cells (Figure 4D). To deeply assess the underlying mechanisms, gene expression assay was performed to evaluate the mRNA expression of chemokines and their relevant receptors. Multiple chemokines, including IP-10, KC, MCP-1, MDC, MIG, MIP, RANTES, and receptors, including CCR2, CCR4, CCR5, CCR6, CCR9, CXCR2, CXCR3 were significantly elevated in the process of UC (Figure 4G). Treatment with apremilast inhibited the expression levels, which were consistent with immunofluorescent assays (Figure 4F, G).

Apremilast inhibited ex vivo proliferation and cytokines production from MLNs

Inspired from the mucosal immunity in the gut tract interfered by apremilast, we cultured mouse MLN cells in the presence or absence of mitogens *ex vivo*. As expected, the proliferation of $CD4^+$ T cells, purified from MLN cells, was reduced in mice that received apremilast under exposure to anti-CD3 plus CD28 antibodies (Figure 5A). In step with proliferation capacity, the release of multiple cytokines IFN-γ, IL-2, IL-10, and IL-17A from $CD4^+$ T cells were also decreased in the apremilast-treated group (Figure 5B). For the whole MLN cells, it was observed that proliferations were reduced in the apremilast groups in the presence of either anti-CD3 antibodies (Figure 5C) or LPS (Figure 5E). TCR stimulation led to robust cytokines release from MLN cells in the vehicle group, to some extent, apremilast drove the cytokines level, including IFN-γ, IL-2, IL-6, IL-10, and IL-17A alike the normal groups (Figure 5D). Moreover, MLN cells from DSS-treated mice were strongly activated by LPS induction, with high production of IFN-γ, IL-6, IL-10, and IL-12p40. However, a relative low secretion of IFN-γ, IL-6, and IL-12p40, not IL-10, was detected in the apremilast group (Figure 5F). Furthermore, the baseline proliferation and cytokines release from $CD4^+$ T cell and whole MLN cells were also reduced associated with apremilast treatment (Supporting Information Figure S4).

Apremilast downregulated the expression of isoform of PDE4 and subsequently activated the PKA-CREB pathway

Previously, gene expression assay of PDE4 isoforms (A, B, C, and D) in peripheral blood mononuclear cells (PBMCs) from patients with Crohn′s disease showed that PDE4C mRNA was preferentially overexpressed versus normal individuals (Schafer *et al.*, 2016). We first measured the expression of four PDE4 isoforms in the colon tissue from murine UC. As shown in Figure 6A, PDE4A, 4B, 4D were remarkedly upregulated while PDE4C exhibited little change in DSS-treated mice. Apremilast deceased both the mRNA and protein level of PDE4 isoforms in a similar tendency (Figure 6A, B), which was further supported by immunostaining with PDE4D (Figure 6C). Next, we determined whether apremilast showed effects on the downstream signaling mediated by PDE4. The results demonstrated that

apremilast could reverse the DSS-caused decrease in the expression of exchange protein 1 directly activated by cAMP (Epac1), Epac2, and phosphor-CREB, meanwhile, apremilast could also upregulate the protein level of Rap1 without any effects on the expression of CREB and PKA (Figure 6B, D).

Apremilast restrained the activation of NF-κB, MAPK, PI3K-AKT-mTOR, JAK-STAT-SOCS mediated-signaling pathway

PDE4 mediated PKA-CREB signaling are closely related to MAPK, NF-κB pathways in diverse inflammatory disease (Li *et al.*, 2018). Western blot assay showed that DSS treatment increased the phosphorylation of p38, ERK, JNK, and MEK1/2; notably, apremilast blocked the phosphorylation of p38, ERK, JNK, and MEK1/2 (Figure 6F). With regards to the NF-κB pathway, the phosphorylation of IκBα and subunit p65 of NF-κB were increased markedly upon DSS treatment, these effects were reversed by apremilast treatment (Figure 6F), which were further confirmed in the immunohistochemical analysis (Figure 6C). Apremilast could also decrease the overexpression of MyD88 and HMGB1, caused by DSS induction (Figure 6F). Moreover, apremilast showed suppressive effects on the phosphorylation of STAT1, STAT3, STAT5, and STAT6 via increasing SOCS3 expression, whereas, it seemed that STAT4 phosphorylation were slightly affected after apremilast treatment (Figure 6E). Strikingly, apremilast retrained the activation of PI3K-mTOR pathway, manifested with phosphorylation of PI3K, AKT, and mTOR (Figure 6G).

Apremilast suppressed LPS-stimulated inflammatory responses through PKA-CREB signaling pathway in macrophages

We additionally corroborate the effect of apremilast on activation of cAMP-PKA-CREB pathway *in vitro*. We introduced RAW264.7 cells, a murine macrophage cell line, and BMDMs with or without LPS challenge. As shown in Figure 7A, apremilast significantly inhibited the production of TNF-α, whereas, increased the production of IL-10 in a concentration-dependent manner. In accordance with the results in Figure 6B, apremilast elevated the cellular level of cAMP in BMDMs and RAW264.7 cells (Supporting Information Figure S5) and subsequently promoted phosphorylation of CREB with no change on the

expression of total CREB protein (Figure 7B). The results were further confirmed in immunofluorescent observation of phosphor-CREB (Figure 7C). Although there were some differences between RAW264.7 cells and BMDMs, the cAMP elevation and CREB phosphorylation were counteracted in the presence of H89, a specific PKA inhibitor, with no effect on the expression of PKA (Figure 7D-G). In agreement with H89 intervention, the similar findings were observed when knock-down the expression of catalytic subunit of PKA using siRNA silence (Figure 7E, F and Supporting Information Figure S6). However, apremilast and forskolin, an adenylyl cyclase activator, showed synergistic effects both in RAW264.7 cells and BMDMs, manifesting with enhancive the elevation of cellular cAMP and CREB phosphorylation (Figure 7D-G). Further biological assay on TNF-α release also displayed the antagonistic effects between apremilast and PKA inhibitors and the synergistic effects between apremilast and adenylyl cyclase inhibitors (Figure 7H, I).

Discussion

Ulcerative colitis (UC) has become a worldwide challenging disease that strikes at all ages and leads to lifelong morbidity or even lethality (Ng *et al.*, 2018). The high rate of resistance to therapy for UC indicates a notable field of unmet clinical medical needs. Thus, it′s eagerly required for alternative therapeutic strategies. Cytokines are well-known to mediate the intestinal inflammation and targeting for cytokines release have been proven to be useful in clinical application. PDE4 functions as a cellular modulator of cAMP and inhibition of PDE4 is predicted to inhibit a wide array of inflammatory cytokines (Maurice *et al.*, 2014). Over the past decades, various PDE4 inhibitors, including rolipram, roflumilast and tetomilast, have been introduced as new therapeutic attempts for the treatment of UC. Owing to severe side effects, including headache, vomiting, nausea and other gastrointestinal problems, rolipram and tetomilast were abandoned for further clinical practice (Spadaccini *et al.*, 2017). Roflumilast, approved for treating asthma and chronic obstructive pulmonary disease, has been previously shown to ameliorate the morphological and biochemical alterations in DSS-induced colitis (El-Ashmawy *et al.*, 2018). By contrast to roflumilast, another PDE4 inhibitor, apremilast, was approved in 2014 for psoriasis and psoriatic arthritis (Chiricozzi *et al.*, 2016). Recently, a phase 2, multicenter, randomized, double-blind, placebo-controlled, parallel-group study was designed to evaluate the clinical efficacy, safety and tolerability of apremilast in patients with active UC; Whereas, there have been none preclinical research on inflammatory colitis published by now. (Li *et al.*, 2018). The present aimed to investigate the efficacy and underlying mechanisms of apremilast in attenuating DSS-induced murine UC. Our results demonstrated that oral administration of apremilast exerted protective effects by interfering with mucosal immunity (Figure 8). Notably, this preclinical research is the first to show therapeutic efficacies of apremilast on intestinal inflammation *in vivo*.

Chemically induced colitis models could mimic some key immunological and histopathological features of UC in humans. Oral administration of the sulfated polysaccharide DSS to mice via drinking water result in severe colitis characterized by weight loss, bloody diarrhea, ulcer formation and infiltrations with inflammatory cells, which

are similar to the manifestations in UC patients. DSS-induced colitis model is widely used preclinically due to its reproducibility, simplicity and controllability (Chassaing *et al.*, 2014). The mechanism by which DSS causes intestinal inflammation is closely associated to the epithelial monolayer damage and abnormal dissemination of proinflammatory contents into the colon mucosa. In our research, apremilast could significantly ameliorate the clinical features of UC, including body weight loss, colon shortening, hematochezia, and diarrhea. Accompanied by intestinal tract bleeding and severe inflammation, serum biochemical parameters were aberrant with loss of ALB, decreased ALP activity, and dyslipidemia (Vermeire *et al.*, 2006); abnormal oxidative stress causes destructions of the mucosal layer in the gut tract and barrier invasion in the initiation and exacerbation of UC (Tian *et al.*, 2017). Apremilast notably alleviated the local and systemic inflammation caused by DSS, as described in the results. Intestinal fibrosis, commonly resulting from epithelial-to-mesenchymal and endothelial-to-mesenchymal transitions, represents an inevitable complication of UC and CD (Rieder *et al.*, 2008). It has been reported previously that in mucosal biopsies from healthy donors and IBD patients, OSM and OSMR expression are closely correlated with high expression of Col1a1, FAP, PDPN and ICAM1, which display the critical pathology in tissue fibrosis (West *et al.*, 2017). In DSS-induced murine UC model, we found these genes were highly expressed in the colon and inhibition of PDE4 exerted inhibition on intestinal fibrosis attributing to suppression of these genes.

The intestinal mucosal barrier plays an essential role in protecting the homeostasis against the chaotic invasion of multiple antigens from outside environment (Turner, 2009; Martini *et al.*, 2017). Genome-wide association studies (GWAS) have identified several UC-susceptible genes involved in intestinal barrier function, including HNF4, CDH1, and LAMB1 (Oshima *et al.*, 2016). Tight junctions are the constitutive structural component in epithelial cells. The in vivo imaging with FITC-dextran revealed apremilast protected the barrier function from DSS-caused damage. Furthermore, the reduction of tight junction proteins was reversed markedly when mice were administrated with apremilast. Besides, increasing studies suggested that TNF-α driven overexpression of gut matrix

metalloproteinase (MMP), especially MMP3, mainly contributed to the colonic damage, leukocyte accumulation, excessive cytokines production and fistula formation in UC (Naito *et al.*, 2005). In the cultured lamina propria mononuclear cells (LPMCs), apremilast could apparently suppress TNF-α and MMP3 production (Gordon *et al.*, 2009).

Although the etiology and pathogenesis of UC remains elusive, the intestine integrity and its immune system have been proven to maintain tolerance to various inflammatory conditions, in which intestinal epithelial cells, macrophages, dendritic cells, adaptive immune cells, and the newly identified innate lymphoid cells refer to the characteristic importance for immune functions in mucosa (Cader *et al.*, 2013). Linked with numerous pathogenetic triggers in UC, the damage appears to the intestinal epithelial cells, leading to barrier function disruption (Figure 3). As highlighted in Figure 8, once disturbance of epithelial integrity, immune cells expressing high levels of inflammatory mediators and chemokines receptor infiltrate to mucosal layers (Zimmerman *et al.*, 2008; Atreya *et al.*, 2010). During the progression of UC, both innate and adaptive immune system are overactivated (Steinbach *et al.*, 2014); In the inflamed tissue, we observed the increased populations of antigen-presenting cells, neutrophils, γδT cells and IL-17-producing cells, which contributed to intestinal mucosal inflammation (Xu *et al.*, 2014). Moreover, the results from *ex vivo* study indicated that the $CD4^+$ T cells purified from MLNs in apremilast-treated mice manifested with weaker immune activity towards specific antigens than that in DSS-treated mice (Figure 5). Our research demonstrated that PDE4 inhibition could interfere with mucosal immunity, manifesting with inhibition of immune cells infiltration, chemokines and chemokine receptor expression, and reduction of the reactivity of immune cells.

PDE4 act as a proinflammatory enzymes targeting for degradation of cAMP, which is well-established as a potent regulator in both innate and adaptive immune cell functions (Raker *et al.*, 2016). Previous report suggested gene expression patterns of PDE4 isoforms in PBMC from healthy individuals and from patients with various immune-mediated or inflammatory diseases including psoriasis, rheumatoid arthritis, idiopathic pulmonary fibrosis, sarcoidosis, scleroderma, Crohn's disease, and systemic lupus erythematosus. PDE4B and

PDE4D were increased at the mRNA level in psoriatic patients; preferentially, PDE4C was overexpressed in patients with Crohn's disease (Schafer *et al.*, 2016). However, there are little researches about the PDE4 isoforms expression in UC. We first determined the PDE4 isoforms in the colon tissue of DSS colitis by RT-qPCR, western blot and immunohistochemical analysis. Strikingly, among four isoforms, PDE4D showed the highest level of expression and the next is PDE4A, PDE4B, and PDE4C. Further investigations are required to measure the expression level of PDE4 isoforms in the PBMC or colon biopsies of UC patients. Moreover, DSS treatment remarkedly led to overexpression of PDE4A, 4B and 4D, not PDE4C yet. Delicate interaction of cAMP, PKA and Epac with PDE4 contribute to the formation of cAMP signalosomes (Maurice *et al.*, 2014). Increasing studies demonstrated that inhibition of PDE4 could result in accumulation of cellular cAMP, and then activate PKA and Epac-dependent pathway in a spatial and temporal manner (Cheng *et al.*, 2008). PKA is composed of two separate subunits, namely catalytic and regulatory subunits. Upon cAMP elevation, the free catalytic subunit is activated and subsequently affect a range of diverse cytoplasmic and nuclear transcriptional factors, including CREB, CREM and ATF-1, which contribute to the anti-inflammation effects in inflammatory conditions (Abdulrahim *et al.*, 2015). This bioactivity was confirmed in our study on RAW264.7 and BMDMs using PKA inhibitor or siRNA targeting for the silence of catalytic subunit of PKA. Furthermore, Epac has been identified as another family of cAMP sensor protein. Epac proteins highly specific for binding to cAMP and activate the small GTPases Rap1, which plays an important role in the formation of cell-cell junctions and promotes the barrier function (Cheng *et al.*, 2008). In consistent with overexpression of PDE4, our results revealed a reduction of Epac1, Epac2 and phosphor-CREB in DSS-induced UC and PDE4 inhibition with apremilast could dramatically downregulate the expression of PDE4 isoforms and increase the expression of Epac1, Epac2 and phospho-CREB. Meanwhile, colon Rap1 protein was activated in the presence of PDE4 inhibition, which accounted for the protective effects on the epithelial barrier. Alternatively, Epac activation could restrict the actions of inflammatory cytokines IL-6 by means of induction of SOCS3 and therewith negative feedback inhibit JAK-STAT

signaling (Parnell *et al.*, 2015). As observed, apremilast increased the expression SOCS3 and inhibited the phosphorylation of STATs. On the other hand, it has been concluded that PDE4 inhibition by apremilast lead to indirect inhibition of MAPK, NF-κB, and PI3K-mTOR pathway, which are involved in the activation of innate and adaptive immunity (Hernandez-Florez *et al.*, 2016).

In conclusion, the current results demonstrated that oral administration of apremilast exerted protective effects in experimental colitis through interfering with mucosal immunity, which provided evidence to illustrate the pathological role of PDE4 in intestinal inflammation. Accordingly, the efficacies are closely associated with PDE4 inhibition in modulating cAMP-mediated PKA-CREB and Epac-Rap1 pathway, which subsequently engage in the MAPK, NF-κB, PI3K-mTOR, and JAK-STAT-SOCS3 signaling pathways. Our study indicates the possibility of a similar therapeutic capacity of PDE4 intervention in UC patients.

References

Abdulrahim H, Thistleton S, Adebajo AO, Shaw T, Edwards C, Wells A (2015). Apremilast: a PDE4 inhibitor for the treatment of psoriatic arthritis. *Expert opinion on pharmacotherapy* **16**(7)**:** 1099-1108.

Alexander SP, Kelly E, Marrion NV, Peters JA, Faccenda E, Harding SD, *et al.* (2017). THE CONCISE GUIDE TO PHARMACOLOGY 2017/18: Overview. *British journal of pharmacology* **174 Suppl 1:** S1-s16.

Atreya R, Neurath MF (2010). Chemokines in inflammatory bowel diseases. *Digestive diseases* **28**(3)**:** 386-394.

Banner KH, Trevethick MA (2004). PDE4 inhibition: a novel approach for the treatment of inflammatory bowel disease. *Trends in pharmacological sciences* **25**(8)**:** 430-436.

Boyapati RK, Rossi AG, Satsangi J, Ho GT (2016). Gut mucosal DAMPs in IBD: from mechanisms to therapeutic implications. *Mucosal immunology* **9**(3)**:** 567-582.

Cader MZ, Kaser A (2013). Recent advances in inflammatory bowel disease: mucosal immune cells in intestinal inflammation. *Gut* **62**(11)**:** 1653-1664.

Chassaing B, Aitken JD, Malleshappa M, Vijay-Kumar M (2014). Dextran sulfate sodium (DSS)-induced colitis in mice. *Current protocols in immunology* **104:** Unit 15 25.

Cheng X, Ji Z, Tsalkova T, Mei F (2008). Epac and PKA: a tale of two intracellular cAMP receptors. *Acta biochimica et biophysica Sinica* **40**(7)**:** 651-662.

Chiricozzi A, Caposiena D, Garofalo V, Cannizzaro MV, Chimenti S, Saraceno R (2016). A new therapeutic for the treatment of moderate-to-severe plaque psoriasis: apremilast. *Expert review of clinical immunology* **12**(3)**:** 237-249.

Curtis MJ, Alexander S, Cirino G, Docherty JR, George CH, Giembycz MA, *et al.* (2018). Experimental design and analysis and their reporting II: updated and simplified guidance for authors and peer reviewers. *British journal of pharmacology* **175**(7)**:** 987-993.

Curtis MJ, Bond RA, Spina D, Ahluwalia A, Alexander SP, Giembycz MA, *et al.* (2015). Experimental design and analysis and their reporting: new guidance for publication in BJP. *British journal of pharmacology* **172**(14)**:** 3461-3471.

de Mattos BR, Garcia MP, Nogueira JB, Paiatto LN, Albuquerque CG, Souza CL, *et al.* (2015). Inflammatory Bowel Disease: An Overview of Immune Mechanisms and Biological Treatments. *Mediators of inflammation* **2015:** 493012.

El-Ashmawy NE, Khedr NF, El-Bahrawy HA, El-Adawy SA (2018). Roflumilast, type 4 phosphodiesterase inhibitor, attenuates inflammation in rats with ulcerative colitis via down-regulation of iNOS and elevation of cAMP. *International immunopharmacology* **56:** 36-42.

Gordon JN, Prothero JD, Thornton CA, Pickard KM, Di Sabatino A, Goggin PM, *et al.* (2009). CC-10004 but not thalidomide or lenalidomide inhibits lamina propria mononuclear cell TNF-alpha and MMP-3 production in patients with inflammatory bowel disease. *Journal of Crohn's & colitis* **3**(3)**:** 175-182.

Gupta J, Nebreda AR (2014). Analysis of Intestinal Permeability in Mice. *Bio-protocol* **4**(22)**:** e1289.

Harding SD, Sharman JL, Faccenda E, Southan C, Pawson AJ, Ireland S, *et al.* (2018). The IUPHAR/BPS Guide to PHARMACOLOGY in 2018: updates and expansion to encompass the new guide to IMMUNOPHARMACOLOGY. *Nucleic acids research* **46**(D1)**:** D1091-D1106.

Hartmann G, Bidlingmaier C, Siegmund B, Albrich S, Schulze J, Tschoep K, *et al.* (2000). Specific type IV phosphodiesterase inhibitor rolipram mitigates experimental colitis in mice. *The Journal of pharmacology and experimental therapeutics* **292**(1)**:** 22-30.

Hernandez-Florez D, Valor L (2016). Selective Phosphodiesterase Inhibitors: A New Therapeutic Option in Inflammation and Autoimmunity. *Reumatologia clinica* **12**(6)**:** 303-306.

Ichikawa H, Okamoto S, Kamada N, Nagamoto H, Kitazume MT, Kobayashi T, *et al.* (2008). Tetomilast suppressed production of proinflammatory cytokines from human monocytes and ameliorated chronic colitis in IL-10-deficient mice. *Inflammatory bowel diseases* **14**(11)**:** 1483-1490.

Kielland A, Blom T, Nandakumar KS, Holmdahl R, Blomhoff R, Carlsen H (2009). In vivo imaging of reactive oxygen and nitrogen species in inflammation using the luminescent probe L-012. *Free radical biology & medicine* **47**(6)**:** 760-766.

Kilkenny C, Browne W, Cuthill IC, Emerson M, Altman DG (2010). Animal research: reporting in vivo experiments: the ARRIVE guidelines. *British journal of pharmacology* **160**(7)**:** 1577-1579.

Li H, Zuo J, Tang W (2018). Phosphodiesterase-4 Inhibitors for the Treatment of Inflammatory Diseases. *Frontiers in pharmacology* **9**.

Martini E, Krug SM, Siegmund B, Neurath MF, Becker C (2017). Mend Your Fences: The Epithelial Barrier and its Relationship With Mucosal Immunity in Inflammatory Bowel Disease. *Cellular and molecular gastroenterology and hepatology* **4**(1)**:** 33-46.

Maurice DH, Ke H, Ahmad F, Wang Y, Chung J, Manganiello VC (2014). Advances in targeting cyclic nucleotide phosphodiesterases. *Nature reviews. Drug discovery* **13**(4)**:** 290-314.

McGrath JC, Lilley E (2015). Implementing guidelines on reporting research using animals (ARRIVE etc.): new requirements for publication in BJP. *British journal of pharmacology* **172**(13)**:** 3189-3193.

Naito Y, Yoshikawa T (2005). Role of matrix metalloproteinases in inflammatory bowel disease. *Molecular aspects of medicine* **26**(4-5)**:** 379-390.

Ng SC, Shi HY, Hamidi N, Underwood FE, Tang W, Benchimol EI, *et al.* (2018). Worldwide incidence and prevalence of inflammatory bowel disease in the 21st century: a systematic review of population-based studies. *Lancet (London, England)* **390**(10114)**:** 2769-2778.

Oshima T, Miwa H (2016). Gastrointestinal mucosal barrier function and diseases. *Journal of gastroenterology* **51**(8)**:** 768-778.

Parnell E, Palmer TM, Yarwood SJ (2015). The future of EPAC-targeted therapies: agonism versus antagonism. *Trends in pharmacological sciences* **36**(4)**:** 203-214.

Raker VK, Becker C, Steinbrink K (2016). The cAMP Pathway as Therapeutic Target in Autoimmune and Inflammatory Diseases. *Frontiers in immunology* **7:** 123.

Rieder F, Fiocchi C (2008). Intestinal fibrosis in inflammatory bowel disease - Current knowledge and future perspectives. *Journal of Crohn's & colitis* **2**(4)**:** 279-290.

Sartor RB (2006). Mechanisms of disease: pathogenesis of Crohn's disease and ulcerative colitis. *Nature clinical practice. Gastroenterology & hepatology* **3**(7)**:** 390-407.

Schafer PH, Parton A, Gandhi AK, Capone L, Adams M, Wu L, *et al.* (2010). Apremilast, a cAMP phosphodiesterase-4 inhibitor, demonstrates anti-inflammatory activity in vitro and in a model of psoriasis. *British journal of pharmacology* **159**(4)**:** 842-855.

Schafer PH, Truzzi F, Parton A, Wu L, Kosek J, Zhang LH, *et al.* (2016). Phosphodiesterase 4 in inflammatory diseases: Effects of apremilast in psoriatic blood and in dermal myofibroblasts through the PDE4/CD271 complex. *Cellular signalling* **28**(7)**:** 753-763.

Spadaccini M, D'Alessio S, Peyrin-Biroulet L, Danese S (2017). PDE4 Inhibition and Inflammatory Bowel Disease: A Novel Therapeutic Avenue. *International journal of molecular sciences* **18**(6).

Speca S, Giusti I, Rieder F, Latella G (2012). Cellular and molecular mechanisms of intestinal fibrosis. *World journal of gastroenterology* **18**(28)**:** 3635-3661.

Steinbach EC, Plevy SE (2014). The role of macrophages and dendritic cells in the initiation of inflammation in IBD. *Inflammatory bowel diseases* **20**(1)**:** 166-175.

Suzuki K, Sun X, Nagata M, Kawase T, Yamaguchi H, Sukumaran V, *et al.* (2011). Analysis of intestinal fibrosis in chronic colitis in mice induced by dextran sulfate sodium. *Pathology international* **61**(4)**:** 228-238.

Tian T, Wang Z, Zhang J (2017). Pathomechanisms of Oxidative Stress in Inflammatory Bowel Disease and Potential Antioxidant Therapies. *Oxidative medicine and cellular longevity* **2017:** 4535194.

Turner JR (2009). Intestinal mucosal barrier function in health and disease. *Nature reviews. Immunology* **9**(11)**:** 799-809.

Uhlig HH, Coombes J, Mottet C, Izcue A, Thompson C, Fanger A, *et al.* (2006). Characterization of Foxp3+CD4+CD25+ and IL-10-Secreting CD4+CD25+ T Cells during Cure of Colitis. *The Journal of Immunology* **177**(9)**:** 5852-5860.

Vermeire S, Van Assche G, Rutgeerts P (2006). Laboratory markers in IBD: useful, magic, or unnecessary toys? *Gut* **55**(3)**:** 426-431.

Wang L, Llorente C, Hartmann P, Yang AM, Chen P, Schnabl B (2015). Methods to determine intestinal permeability and bacterial translocation during liver disease. *Journal of immunological methods* **421:** 44-53.

West NR, Hegazy AN, Owens BMJ, Bullers SJ, Linggi B, Buonocore S, *et al.* (2017). Oncostatin M drives intestinal inflammation and predicts response to tumor necrosis factor-neutralizing therapy in patients with inflammatory bowel disease. *Nature medicine*.

Wirtz S, Popp V, Kindermann M, Gerlach K, Weigmann B, Fichtner-Feigl S, *et al.* (2017). Chemically induced mouse models of acute and chronic intestinal inflammation. *Nature protocols* **12**(7)**:** 1295-1309.

Woting A, Blaut M (2018). Small Intestinal Permeability and Gut-Transit Time Determined

with Low and High Molecular Weight Fluorescein Isothiocyanate-Dextrans in C3H Mice. *Nutrients* **10**(6).

Xu XR, Liu CQ, Feng BS, Liu ZJ (2014). Dysregulation of mucosal immune response in pathogenesis of inflammatory bowel disease. *World journal of gastroenterology* **20**(12)**:** 3255-3264.

Ying W, Cheruku PS, Bazer FW, Safe SH, Zhou B (2013). Investigation of macrophage polarization using bone marrow derived macrophages. *Journal of visualized experiments : JoVE*(76).

Zimmerman NP, Vongsa RA, Wendt MK, Dwinell MB (2008). Chemokines and chemokine receptors in mucosal homeostasis at the intestinal epithelial barrier in inflammatory bowel disease. *Inflammatory bowel diseases* **14**(7)**:** 1000-1011.

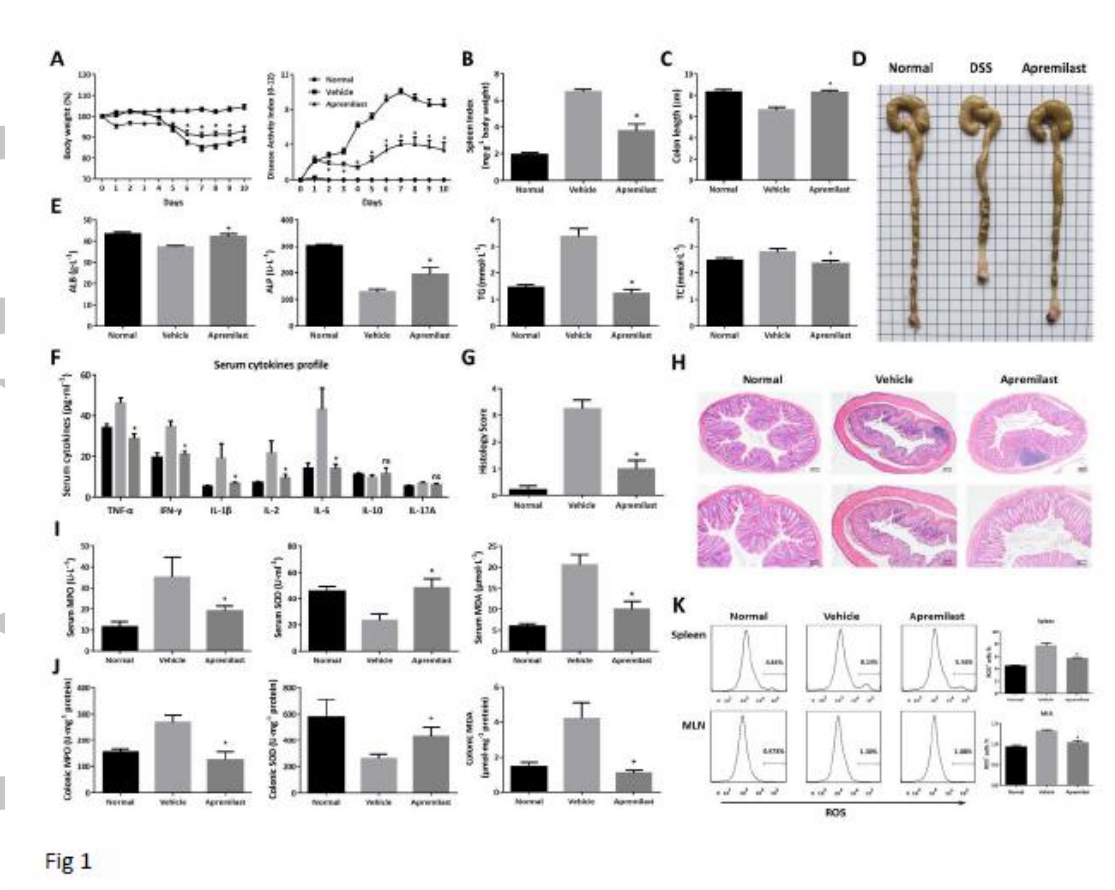

Fig 1

Figure 1. Apremilast ameliorated DSS-induced inflammation and oxidative stress in colitic mice. Murine colitis was established with 3% DSS for 7 days and drinking water for succedent 4 days. (A) Body weight expressed as percentage of initial weight and Disease Activity Index (DAI) mean values assigned based on the criteria described in Table1. (B) Spleen index calculated by spleen weight (mg)/body weight (g). (C) Colon length. (D) Representative colon images. (E) Serum biochemical indices including ALB, ALP, TG and TC. (F) Serum cytokines secretion. (G) Histologic score assigned according to the criteria described in Methods. (H) Representative histological sections of colonic mucosa stained with haematoxylin and eosin (20× and 40× magnification). (I) Serum MPO, SOD and MDA. (J) Colonic MPO, SOD and MDA. (K) Flow cytometry analysis and quantification of ROS production in spleen and mesenteric lymph node cells. Data were shown as means±SEM; n=8 mice per group. *$p<0.05$, significantly different from vehicle group.

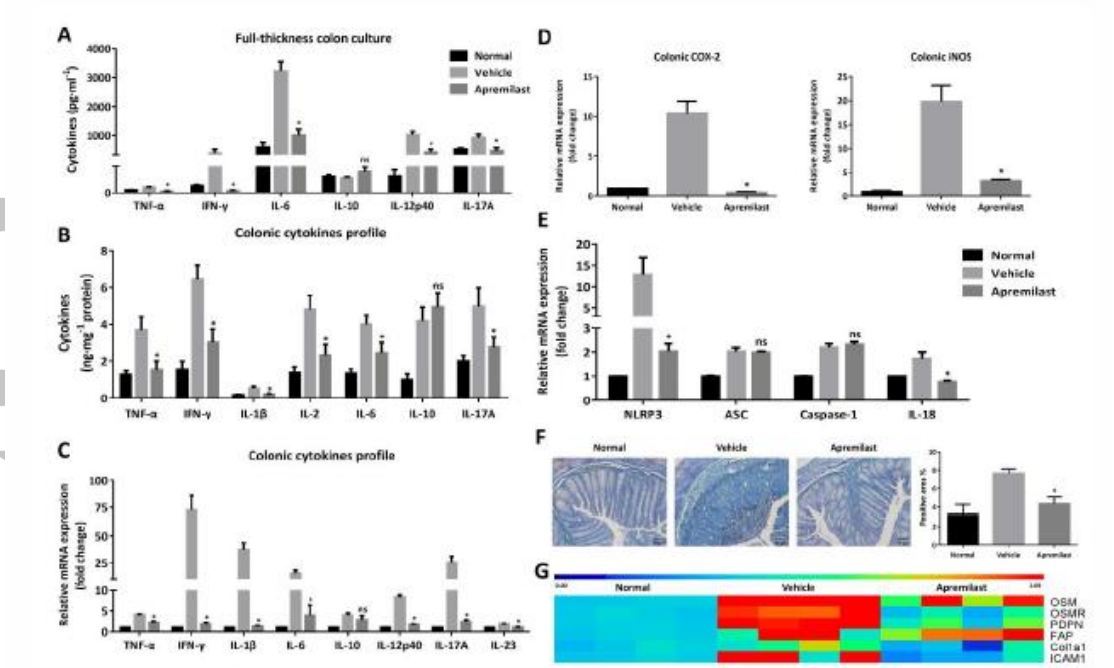

Fig 2

Figure 2. Apremilast suppressed the production of inflammatory mediators and colonic fibrosis in colitic mice. (A) Cytokines production profile in the full-thickness colon culture. (B) Protein levels of cytokines in the tissue homogenates. (C) The mRNA expression of cytokines in colon. (D) The mRNA expression of iNOS and COX-2 in colon. (E) The mRNA expression of inflammasome-related genes in colon. (F) Representative sections and quantification with positive area (%) of colonic mucosa with masson staining (100× magnification). (G) The mRNA expression of fibrosis-related genes in colon. Data were shown as means±SEM; n=8 per group. *$p<0.05$, significantly different from vehicle group.

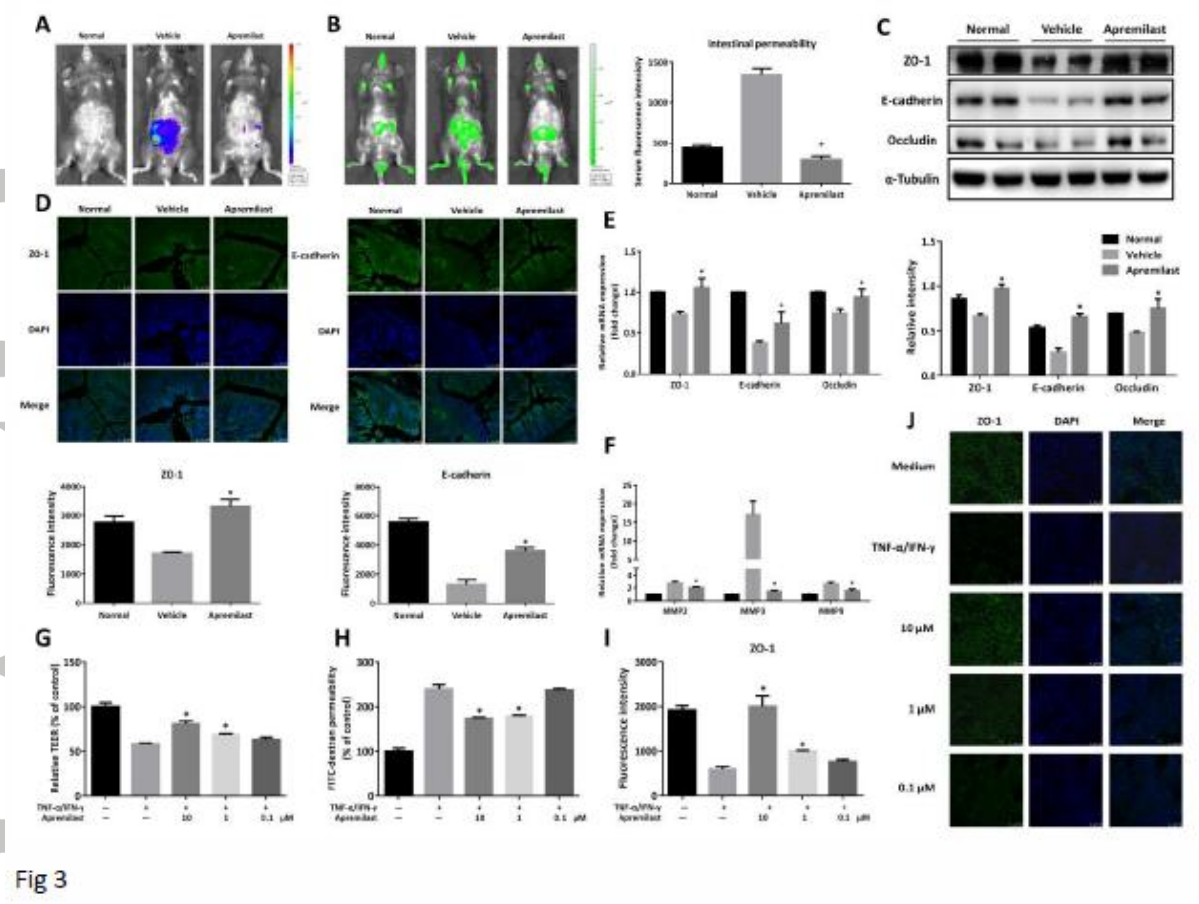

Fig 3

Figure 3. Apremilast protected the intestinal epithelial barrier function and prevented cytokine-induced epithelial barrier disruption. (A) Bioluminescent imaging with L-012 sodium was obtained under isoflurane anesthesia under an IVIS Spectrum CT system. (B) Fluorescence imaging with FITC-dextran administration (left) and serum fluorescence intensity of FITC-dextran (right) were measured. (C) The expression of tight junction-associated proteins (ZO-1, E-cadherin and occludin) detected by western blot and α-Tubulin was used as a loading control. (D) Colonic tissues were immunofluorescence stained with ZO-1 and E-cadherin, and the nuclei were stained with DAPI. (E) The mRNA level of tight junction-associated proteins. (F) The mRNA expression of MMP2, MMP3 and MMP9. (G) Barrier function was measured as TEER in Caco-2 cell monolayers primed by TNF-α and IFN-γ. (H) FITC-dextran permeability in cytokines-induced Caco-2 cells. (I) Quantification of fluorescence intensity of ZO-1 in Caco-2 cells. (J) Representative image of immunofluorescence staining of ZO-1 in Caco-2 cells. Data were shown as means±SEM. (A)-(F), n=8 per group. *p<0.05, significantly different from vehicle group. (G)-(J), n=5.

*p<0.05, significantly different from TNF-α plus IFN-γ treated group.

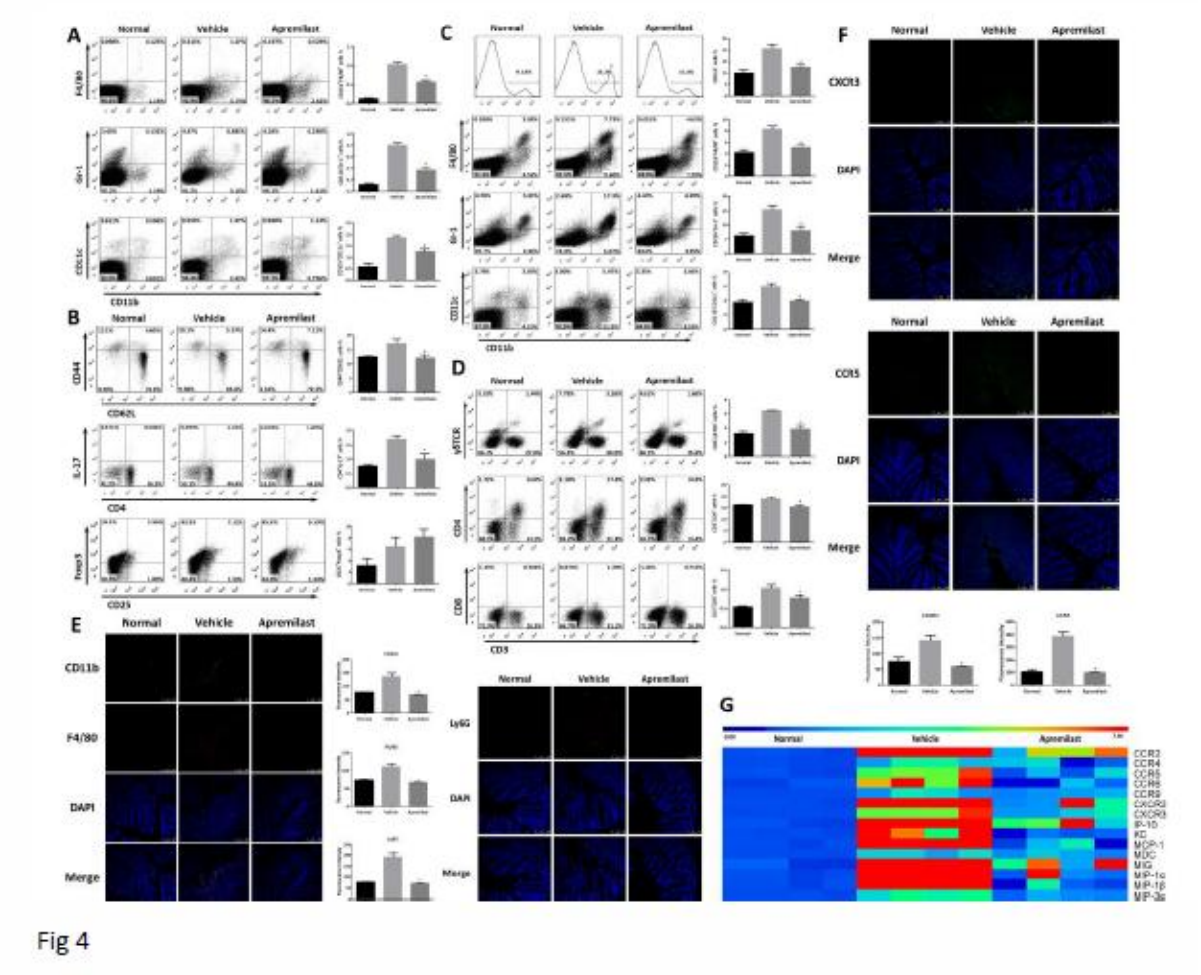

Fig 4

Figure 4. Apremilast regulated the leukocyte populations of mesenteric lymph nodes and lamina propria by suppressing the expression of chemokines and receptor. (A) The percentage of macrophages ($CD11b^+F4/80^+$), neutrophils ($CD11b^+Gr\text{-}1^+$), and dendritic cells ($CD11b^+CD11c^+$) in MLNs. (B) The percentage of naïve T cells ($CD44^-CD62L^+$, gated on $CD3^+CD4^+$), effector T cells ($CD44^+CD62L^-$, gated on $CD3^+CD4^+$), Th17 cells ($CD4^+IL\text{-}17^+$, gated on $CD3^+$), and Treg cells ($CD25^+Foxp3^+$, gated on $CD3^+CD4^+$) in MLNs. (C) The percentage of $CD11b^+$ monocytes, macrophages, neutrophils and dendritic cells in lamina propria. (D) The percentage of $\gamma\delta TCR^+$ T cells, $CD4^+$ T cells, and $CD8^+$ T cells in lamina propria. (E) Colonic tissues were immunofluorescence stained with CD11b, F4/80 and Ly6G, and the nuclei were stained with DAPI. (F) Colonic tissues were immunofluorescence stained with CXCR3 and CCR5. (G) The mRNA expression of chemokines and receptors in colon tissue. Data were shown as the representative images under flow cytometry and immunofluorescence staining. The quantification data were shown as means±SEM; n=8 per

group. *p<0.05, significantly different from vehicle group.

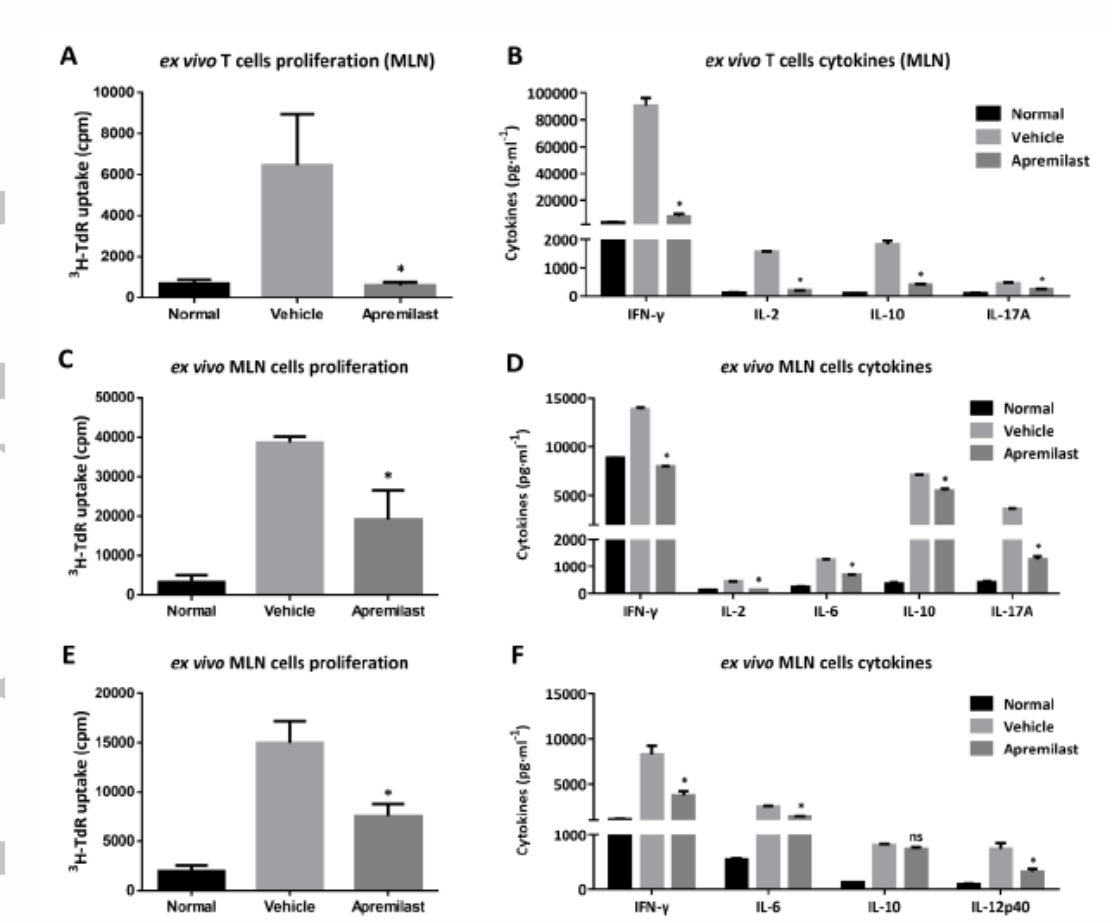

Fig 5

Figure 5. Apremilast inhibited the lymphocyte proliferation and cytokines production upon *ex vivo* stimulation. $CD4^+$ T cells were purified from MLNs and treated with anti-CD3 plus anti-CD28 antibodies to determine the $CD4^+$ T cell proliferation (A) and cytokines production, including IFN-, IL-2, IL-10 and IL-17A (B). (C) The MLN cells proliferation were treated with anti-CD3 antibodies and meanwhile cytokines production (D) were determined. (E) The MLN cells proliferation were treated with LPS and meanwhile cytokines production (F) were determined. Data were shown as means±SEM; n=8 per group. *p<0.05, significantly different from vehicle group.

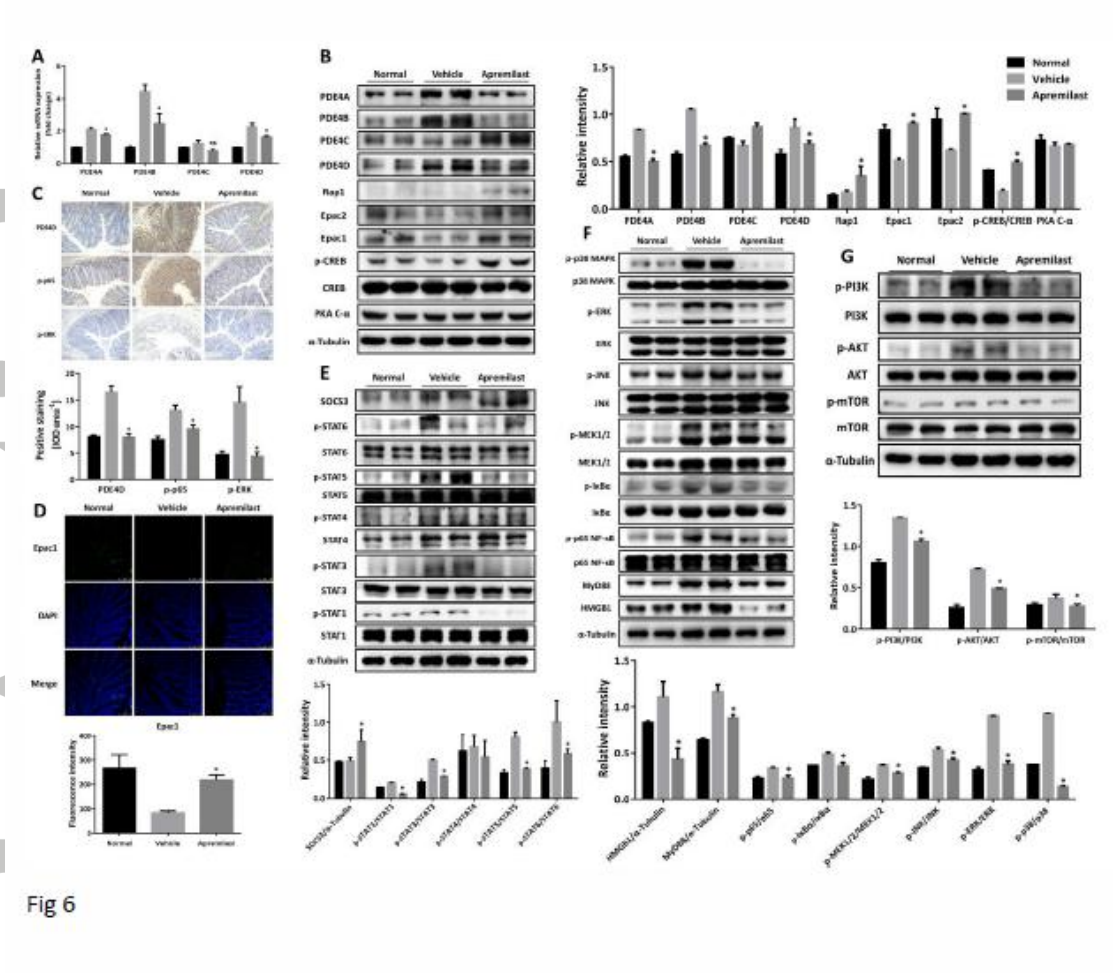

Fig 6

Figure 6. Apremilast inhibited PDE4 expression, activated PKA-CREB and Epac-Rap1 signaling and subsequently interfered with JAK-STAT-SOCS3, PI3K-mTOR, NF-κB and MAPK pathway. (A) The mRNA expression of the isoform of PDE4 in colonic tissue. (B) The expression of the isoform of PDE4 and PKA-CREB signaling-associated proteins. (C) Immunohistochemistry staining of PDE4D, p-p65 and p-REK of colonic tissue. (D) Immunofluorescence staining of Epac1 of colonic tissue. Western blot analysis of JAK-STAT-SOCS3 signaling (E), NF-κB and MAPK-mediated signaling (F) and PI3K-mTOR signaling (G). Data were shown as the representative images under western blot assay and immunohistochemistry staining. The quantification data were shown as means±SEM; n=8 per group. *$p<0.05$, significantly different from vehicle group.

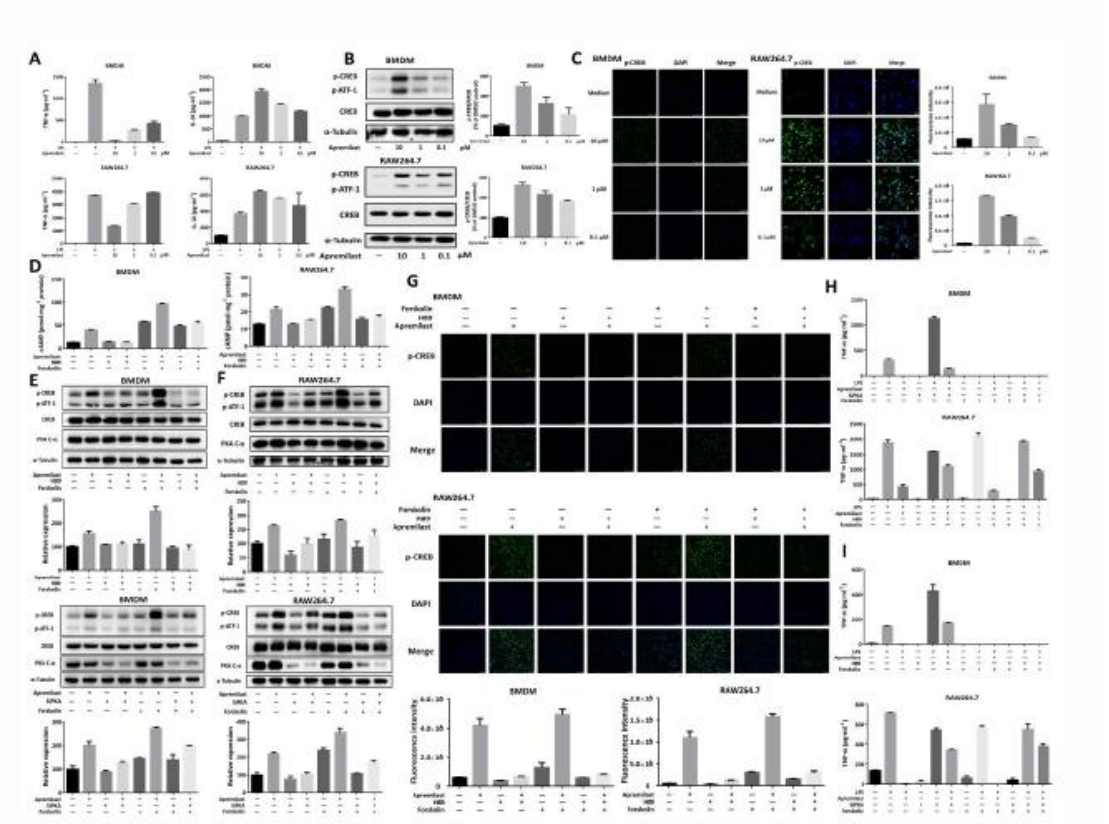

Fig 7

Figure 7. Apremilast suppressed the inflammatory responses in macrophages through PKA-CREB signaling. (A) TNF-α and IL-10 production in LPS-stimulated BMDMs and RAW264.7 cells. (B) The phosphorylation of CREB and ATF-1 upon apremilast treatment determined by western blot. (C) Immunofluorescence staining of phospho-CREB upon apremilast treatment. BMDMs and RAW264.7 cells were treated with 10 μM apremilast, 10 μM H89 (PKA inhibitor) and 10 μM Forskolin, cAMP level (D), phosphorylation of CREB and ATF-1 (upper E, upper F, and G) were measured and TNF-α production were determined upon LPS stimulation (H). BMDMs and RAW264.7 cells were transfected with PKA siRNA and NC SiRNA, then cells were treated with apremilast, H89 and Forskolin. The phosphorylation of CREB and ATF-1 (nether E, nether F) and TNF-α (I) were measured. The quantification data were shown as means±SEM of three independent experiments.

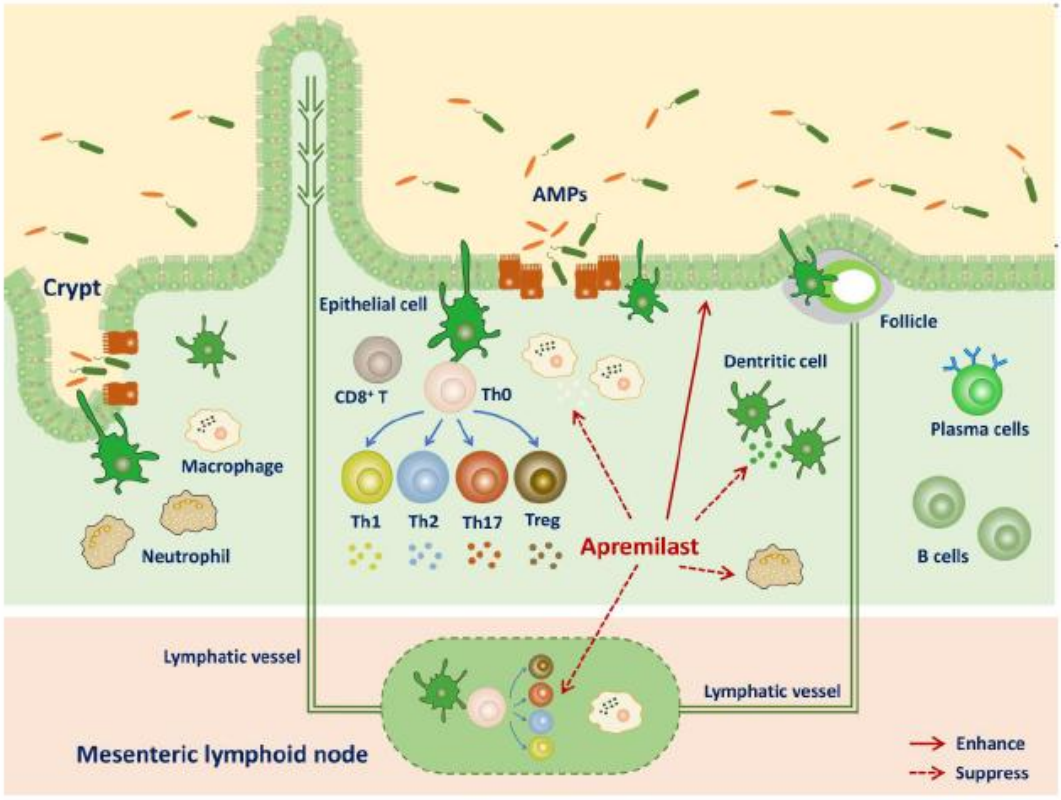

Fig 8

Figure 8. Schematic models of mucosal immunity affected by apremilast to attenuate murine ulcerative colitis.

Table 1. Scoring system for calculating a disease activity index (DAI)

Score	Weight loss	Stool Consistency	Blood
0	None	Normal	Negative hemocult
1	1-5 %	Soft but still formed	Weakly positive hemocult
2	6-10 %	Soft	Positive hemocult
3	11-20 %	Very soft; wet	Blood traces in stool visible
4	> 20 %	Watery diarrhea	Gross rectal bleeding